

Influence of Thermomigration on Lead-Free Solder Joint Mechanical Properties

Mohd F. Abdulhamid

Cemal Basaran¹

e-mail: cjb@buffalo.edu

Electronic Packaging Laboratory,
University at Buffalo,
SUNY,
Buffalo, NY 14260

Thermomigration experiments were conducted to study the change in mechanical properties of 95.5Sn–4Ag–0.5Cu (SAC405) lead-free solder joint under high temperature gradients. This paper presents some observations on samples that were subjected to 1000°C/cm thermal gradient (TG) for 286 h, 712 h, and 1156 h. It was observed that samples subjected to thermal gradient did not develop a Cu₃Sn intermetallic compound (IMC) layer, and we observed disintegration of Cu₆Sn₅ IMC. On the other hand, samples subjected to isothermal annealing exhibited IMC growth. In samples subjected to thermomigration, near the cold side the Cu concentration is significantly higher compared with hot side. Extensive surface hardness testing showed an increase in hardness from the hot to cold sides, which possibly indicates that Sn grain coarsening is in the same direction. [DOI: 10.1115/1.3068296]

Keywords: thermomigration, lead-free, hardness, elastic modulus, grain coarsening

1 Introduction

The insatiable demand for miniaturization of electronics and power electronics increases electrical current density and thermal gradient (TG) in electronic packaging solder joints by orders of magnitude. The high current density and high temperature gradient induce mass migration that degrades the solder joints [1,2]. The two primary mass migration processes that manifest in solder joints subjected to high current density are electromigration and thermomigration [1–8].

When a metal conductor is subject to a high current density, the so-called electron wind transfers part of the momentum to the atoms (or ions) of metal (or alloy) to make the atoms (or ions) move in the direction of the electrons. Electromigration causes atomic accumulation and hillock formation in the anode side, and vacancy condensation and void formation in the cathode side [2,6]. Both hillocks and voids will cause the degradation of the solder joint and eventual failure.

Thermomigration is mass migration that takes place due to high thermal gradients. Thermal gradient can be a result of Joule heating due to a high current density in structures with asymmetric thermal boundaries. This phenomenon is very similar to the Soret effect in fluids. Soret [9] discovered that concentration of a salt solution in a tube with both ends at different temperatures does not remain uniform. The salt was less concentrated on the hot end compared with the cold end. He concluded that a flux of salt was generated by a temperature gradient, which results in a concentration gradient in steady state conditions [10]. Ye et al. [6] showed that the same process also takes place in solder alloy. Research suggests that the effect of thermomigration on solder joint is as serious as that of electromigration [5–8,11].

Thermomigration in PbIn solder was reported by Roush and Jaspal [11] at a temperature gradient of 1200°C/cm. Both In and Pb move in the direction of the thermal gradient, that is, from hot to the cold. Huang et al. [5] investigated thermomigration of SnPb solder alloy at an estimated temperature gradient of 1000°C/cm. They found that Sn moved to the hot end while Pb moved to the

cold end. Ye et al. [6] reported that thermomigration may assist electromigration if the higher temperature side coincides with the cathode side, and counterelectromigration if the hot side is the anode side.

In this paper, thermomigration effects on lead-free solder joints are studied experimentally. High thermal gradients, as high as 1000°C/cm, are applied to SnAgCu solder joints without any current flow. In other words, samples in our experiment are solely subjected to high temperature gradients but not to electrical current. The microstructural changes and growth (IMC) on both sides of the solder joint are observed using scanning electron microscope (SEM) equipped with electron dispersive X-ray (EDX). The hardness properties are measured using nanoindentation method.

2 Experimental Setup

The lead-free solder alloy used in this study is commercially available and the composition by weight is 95.5% Sn, 4.0% Ag, and 0.5% Cu (SAC 405). The solder ball joins two copper plates with dimensions of 19 mm by 38 mm and 0.8 mm thick. The copper plates are polished to a mirrorlike finish to remove any possible oxidation. The plate is then covered with solder mask except at locations where the solder joints are reflowed. Two 1-mm thick glass plates are used as spacers to maintain the gap between the copper plates. The spacer also helps maintain a consistent solder joint height. The solder joints are reflowed using the Joint Electron Device Engineering Council (JEDEC) [12] reflow profile.

Four samples are sandwiched between a lower Al block in contact with a hot plate and an upper Al block in contact with a thermoelectric cooler, as shown in Fig. 1. Every contact surface is coated with thermal grease to maximize heat transfer. The open area between plates and between blocks is insulated to minimize effects from heat radiation and circulating heat flow. The hot side and cold side temperatures are maintained close to 160°C and 50°C in order to achieve a minimum of 1000°C/cm [5] temperature gradient, which has been established to induce thermomigration. At 160°C, a layer of Cu₃Sn should be visible after some time in between the Cu₆Sn₅ layer and copper plate [13] as a result of increased Cu concentration due to copper plate reaction with the Cu₆Sn₅ IMC. Higher temperature gradient results in higher diffusion driving force, while higher temperature results in higher atom

¹Corresponding author.

Contributed by the Electrical and Electronic Packaging Division of ASME for publication in the JOURNAL OF ELECTRONIC PACKAGING. Manuscript received September 25, 2007; final manuscript received April 17, 2008; published online February 11, 2009. Assoc. Editor: Stephen McKeown.

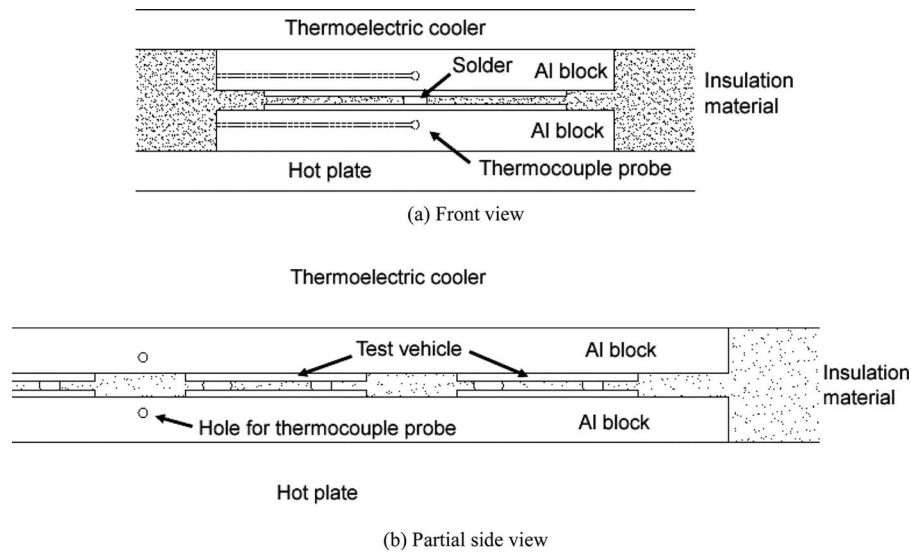


Fig. 1 (a) Front view of the test vehicle sandwiched between heating and cooling plates. (b) Partial side view of test apparatus showing 3 out of 4 possible test vehicles. In both views, the thermocouple probe locations are indicated.

diffusivity rate. A combination of high temperature with high temperature gradient is expected to produce the most detrimental effect.

Thermocouple probes are placed in holes, very close to test vehicle, on the Al blocks, as shown in Fig. 1. The temperatures are recorded every 15 min. Twenty-two samples were tested for up to 1156 h during this project.

3 Sample Preparation

The thermally stressed samples were embedded in epoxy, sliced, and mirror polished to the center section of the joint automated polishing machine with programmable polishing head. The final surface finish was polished using a 0.05 μm silica suspension to ensure accurate nanoindentation test results.

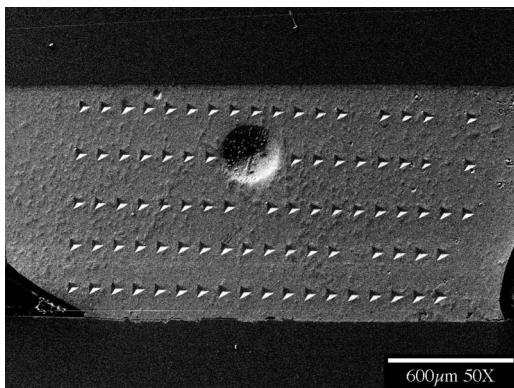


Fig. 2 Indentation marks on tested solder joint. Bottom side is the hot side.

Microstructural morphology and IMC elemental analyses were performed on the prepared samples using backscatter SEM equipped with EDX.

Nanoindentation tests were done using an MTS Nano Indenter[®] XP system with a Berkovich tip at room temperature. Five rows of up to 25 indentations were used to evaluate the solder joint mechanical properties. Each row represents normalized distances of 0.1, 0.3, 0.5, 0.7, and 0.95 from the hot side (bottom side), as shown in Fig. 2.

Nanoindentation hardness measurements were performed using a maximum load of 250 mN and a loading time of 15 s. The contact elastic stiffness is calculated by fitting the upper 50% portion of the unloading data and an assumed value of Poisson's ratio of 0.33. The theory behind surface hardness measurement and elastic modulus calculation is presented in great detail in Ref. [14].

4 Discussion of Observations

4.1 FEM Analysis. The temperatures at the hot and cold sides are relatively constant at approximately 160 °C and 50 °C, respectively, with an error margin of ± 1 °C. Due to the distance of the thermocouples to the solder joint and the difficulty in measuring the temperature at the top and bottom of the solder joint, a 3D finite element method (FEM) heat transfer analysis was used. An eight-node linear heat transfer brick element was utilized, and the thermocouple probe locations were used as thermal boundary conditions. The mesh sensitivity is very low in such a way that a 167% increase in the number of elements results in a 0.2% decrease in temperature. Temperature dependent (between 30 °C and 220 °C, unless otherwise stated) material properties used for the FEM analysis are tabulated in Table 1. The results show that the

Table 1 Material properties used in FEM heat transfer analysis

Material	Density (kg/m ³)	Thermal conductivity (W/m K)	Specific heat (J/kg K)	Reference
Aluminum	2370	$2 \times 10^{-6}T^3 - 0.0024T^2 + 1.0583T + 86$	$-0.001T^2 + 1.2432T + 611.38$	[15]
Copper	8960	$-2 \times 10^{-6}T^3 + 0.0028T^2 - 1.2117T + 571$	$-0.0002T^2 + 0.2843T + 319.43$	[15]
SAC405	7440	57.3 at 25 °C, 33 at 85 °C	220	[16,17]

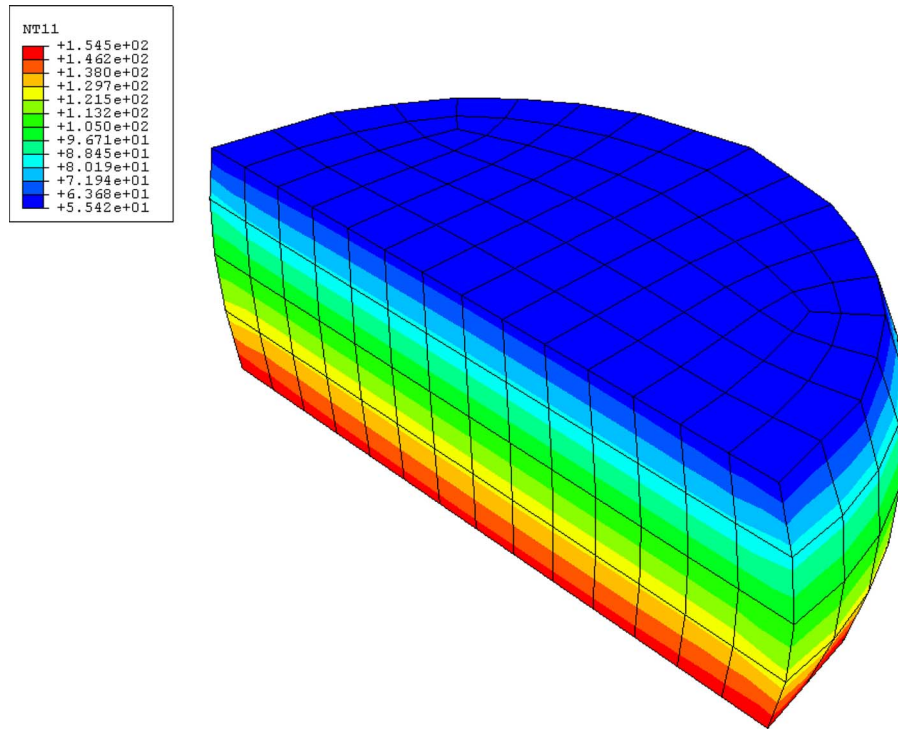


Fig. 3 FEM heat transfer analysis results show that the highest (bottom) temperature is 155°C while the lowest (top) temperature is 55°C, creating a temperature gradient of 1000°C/cm

top and bottom temperatures are 155°C and 55°C, thus creating a temperature gradient of 1000°C/cm (Fig. 3).

4.2 SEM-EDX Observations. The experiments are stopped at 286 h, 712 h, and 1156 h. Samples are cross sectioned and analyzed using SEM and EDX for microstructural and elemental analyses, especially at the hot and cold interfaces. The results are compared with those of isothermally annealed samples of the same stressing time. Isothermal heating took place at 55°C and 170°C, which is almost the same temperature as the cold and hot sides of the test vehicle. Isothermally annealed samples are manufactured the same way as other samples.

The IMC thickness is measured using an image processing software. The software is used to identify and calculate the IMC area enclosed in a square, whose dimension is dependent on the IMC thickness. The thicker the IMC, as in the case of isothermal annealing, the bigger the square is. To reduce the waviness effect, as in the case of the hot side of thermal gradient samples, the square size is reduced to $10 \times 10 \mu\text{m}^2$. The IMC thickness can be determined when the IMC area is known. A minimum of five squares

are used to establish the average IMC thickness.

The Cu_6Sn_5 IMC at both hot and cold sides for flowed (i.e., untested) sample is shown in Fig. 4. The IMC, which provides bonding between solder joint and Cu plates, is planar at both sides. The average thickness of the IMC layer on top and bottom sides are $6.7 \pm 0.6 \mu\text{m}$ and $4.5 \pm 0.4 \mu\text{m}$, respectively. The copper plate/IMC and IMC/solder interfaces for both sides are well defined.

Copper plate/solder joint interface at the colder (top) side after 286 h, 712 h, and 1156 h is shown in Fig. 5, while the hot (bottom) side is shown in Fig. 6. After 286 h of exposure to the thermal gradient, the hot side (Fig. 6) shows a different structure of Cu_6Sn_5 IMC compared with the cold side (Fig. 5).

At the cold side, the plate/IMC interface is relatively flat, while the IMC/solder interface is fingerlike, as outlined in Fig. 5. At both interfaces, a well formed border can be seen between the plate and IMC and between the IMC and solder.

At the hot side, the plate/IMC and IMC/solder interface is irregular and wavy, as outlined in Fig. 6. The Cu_6Sn_5 IMC thick-

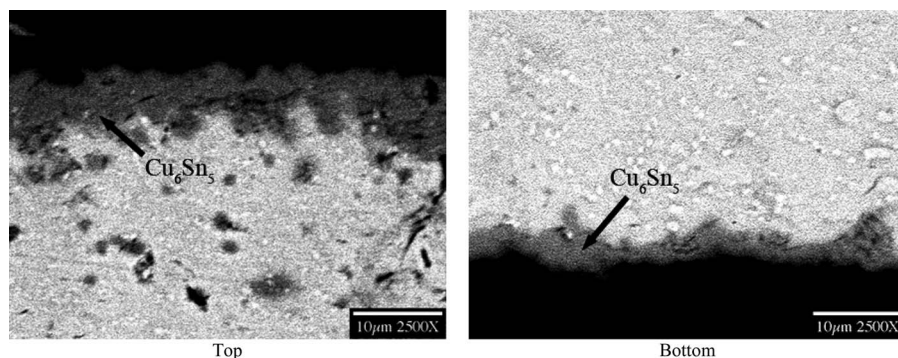


Fig. 4 Copper plate/solder joint interface for the as-flowed sample

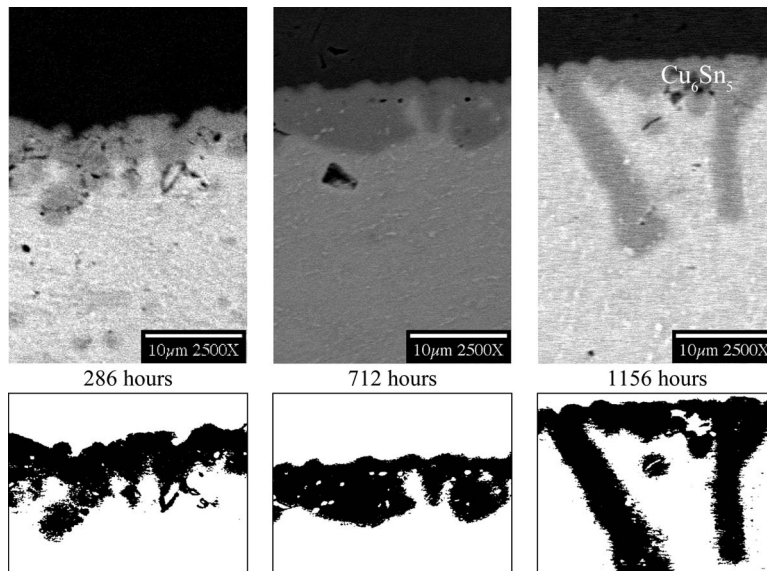


Fig. 5 Cold side copper plate-solder joint interface in thermomigration samples showing no development of Cu_3Sn . Bottom row shows the outline of the Cu_6Sn_5 layer.

ness is nonuniform across the cross section. At some locations, there is no observable IMC layer. The average hot side IMC thickness and its ratio to the initial thickness are determined, as shown in Table 2.

From Table 2, the data scatter increases as annealing time increases, most probably due to the difficulty in measuring the nonuniform and wavy IMC thickness. The nonuniformity and waviness of the IMC for the TG sample after 286 h of annealing is shown in Fig. 7.

Copper plate/solder joint interface at the top side after 286 h, 712 h, and 1156 h for isothermal annealing at 55°C sample is shown in Fig. 8, while at the bottom side for isothermal annealing at 170°C is shown in Fig. 9. Evolution of an additional IMC layer is observed between the Cu_6Sn_5 and Cu plates in 170°C isothermally annealed samples (Fig. 9), for the same testing duration.

The layer is identified as Cu_3Sn . This secondary IMC layer did not form in samples that were subjected to 55°C isothermal annealing and thermal gradient.

After 1156 h, in the samples subjected to the thermal gradient Cu_6Sn_5 the IMC structure at the cold (top) side becomes finger-like, while the IMC at the hot side becomes wavy and thinner. The isothermal samples show an increase in thickness of Cu_6Sn_5 and Cu_3Sn IMC, which does not happen in thermal gradient samples. The ratio of Cu_6Sn_5 to Cu_3Sn remains the same as the initial state. The Cu_6Sn_5 layer thickness is about 2.3 times thicker than Cu_3Sn , as shown in Table 3. The ratio is lower than the value obtained by Grusd [18], of which is 3 after more than 264 h of 150°C isothermal heating. The trend of decreasing ratio as the annealing tem-

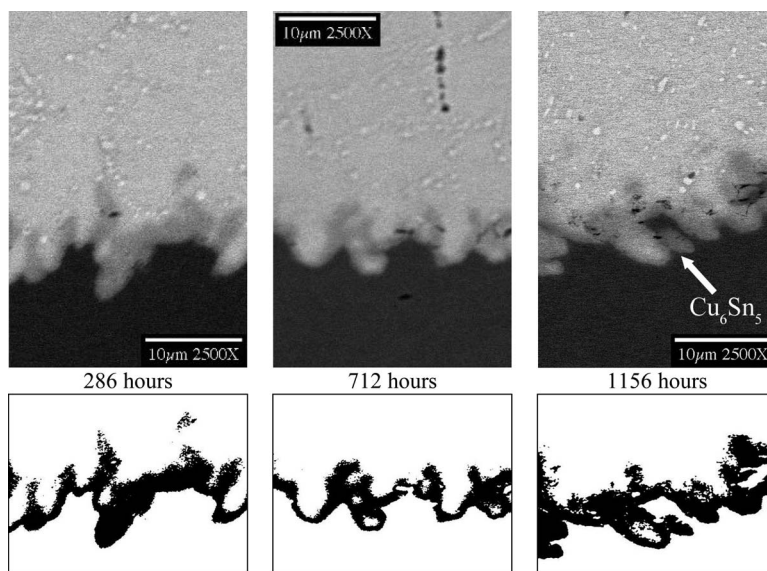


Fig. 6 Hot (bottom) side copper plate-solder joint interface in thermomigration samples showing no development of Cu_3Sn . Bottom row shows the outline of the Cu_6Sn_5 layer.

Table 2 Thickness of IMC on the hot side of thermal gradient samples

Thermal gradient annealing time (h)	Average hot side IMC thickness (μm)	95% confidence interval on thickness (μm)	% thickness of initial
0	4.5 ± 0.4	4.1–4.9	100
286	3.3 ± 0.5	2.9–3.7	73
712	2.8 ± 0.7	2.3–3.4	62
1156	3.1 ± 0.8	2.4–3.8	69

perature increases is in agreement with the findings of Lee et al. [19] (Table 4) for the Sn–3.8Ag–0.7Au solder isothermally annealed for 500 h.

4.3 Nanoindentation Testing. In this study, MTS nanoindenter was used for hardness and modulus measurements, whose details are given in Ref. [14]. In this experiment, the hardness

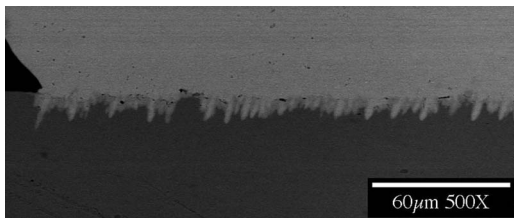


Fig. 7 Hot interface of TG sample after 286 h of annealing showing the nonuniformity and waviness of the IMC

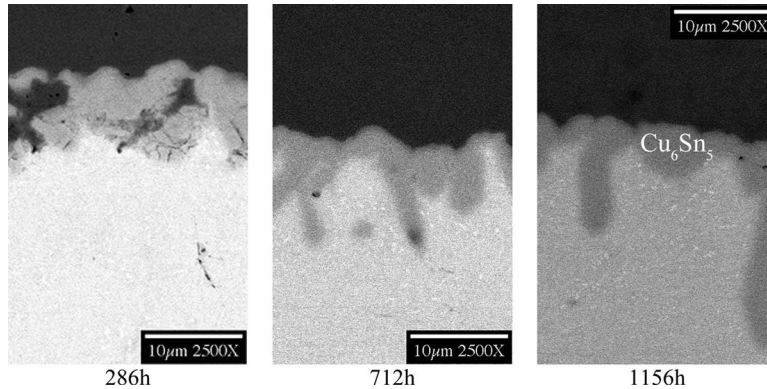


Fig. 8 Top side of isothermal (55 °C) samples showing the development of only the Cu_6Sn_5 IMC

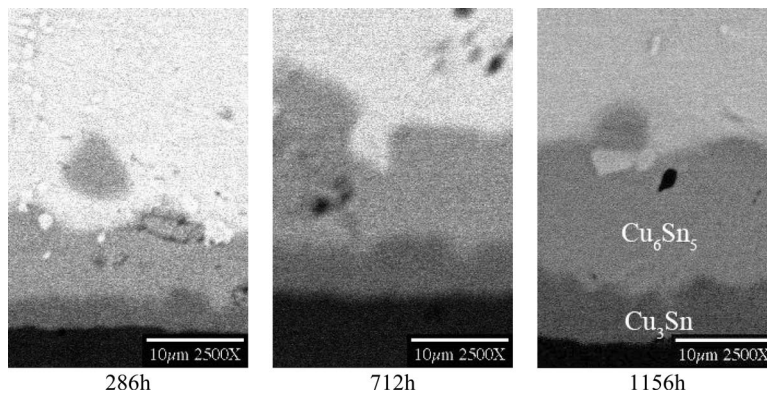


Fig. 9 Bottom side of isothermal (170 °C) samples showing the development of Cu_3Sn IMC between Cu plate and Cu_6Sn_5 IMC

Table 3 IMC thickness for isothermal annealed samples

Isothermal annealing time (h)	Average IMC thickness		
	Cu_6Sn_5 (μm)	Cu_3Sn (μm)	Ratio
0	4.5 ± 0.4	—	—
286	7.8 ± 0.4	3.5 ± 0.3	2.2
712	12.5 ± 0.5	5.5 ± 0.4	2.3
1156	14.8 ± 0.7	6.4 ± 0.6	2.3

measurement and modulus calculation for each indentation is based on a prescribed maximum load of 250 mN after considering the surface area size and number of indentation that needs to be done. A larger load will produce a deeper and larger area of indentation thus limiting the number of indentations that can be done. The average indentation depth due to 250 mN maximum load is $7.5 \mu\text{m}$. The depth is in orders of magnitude smaller than the size of the solder joint in such a way that the measurements are not influenced by the distance from the free edge.

The measurement method uses a series of load/unload cycles for an indentation. The hardness and modulus are determined using the stiffness calculated from the slope of displacement curve (Fig. 10) during each unloading cycle [14]. As shown in Fig. 11, at maximum load, the hardness reaches an asymptotic value, which indicates the actual hardness of the material. In Fig. 12, however, the maximum load has not caused the elastic modulus to reach an asymptotic value. The modulus is not indicative of the actual modulus, but in this experiment it provides comparative moduli across the surface area of the same sample.

Table 4 IMC thickness ratio for Sn-3.8Ag-0.7Au solder isothermally annealed for 500 h at different temperatures. Data from Ref. [19].

Isothermal annealing temperature (°C)	Average IMC thickness		
	Cu ₆ Sn ₅ (μm)	Cu ₃ Sn (μm)	Ratio
125	3.49 ± 0.41	0.73 ± 0.06	4.8
150	4.08 ± 0.35	1.59 ± 0.07	2.6
170	5.38 ± 0.81	3.18 ± 0.15	1.7

A typical hardness measurement and elastic modulus for one row of indentation points are shown in Figs. 11 and 12, respectively. Only the measurement at maximum load is taken into account for this paper. For each test, the number of specimen used ranges from 2 to 4. The numerical data and statistical analysis for Figs. 11 and 12 are presented in the Appendix.

The mean hardness and elastic modulus for every sample versus the distance from the hot side are plotted in Figs. 13 and 14, respectively. Numerical data for both figures are available in the Appendix. The average surface hardness (Fig. 13) from nanoindentation tests shows that the thermal gradient sample hardness increases from the hot to the cold side at a relatively constant rate. The average hardness for the as-flowed samples is shown for ref-

Load-Indentation Depth Curve for Hardness and Modulus Measurement at an Indentation Point

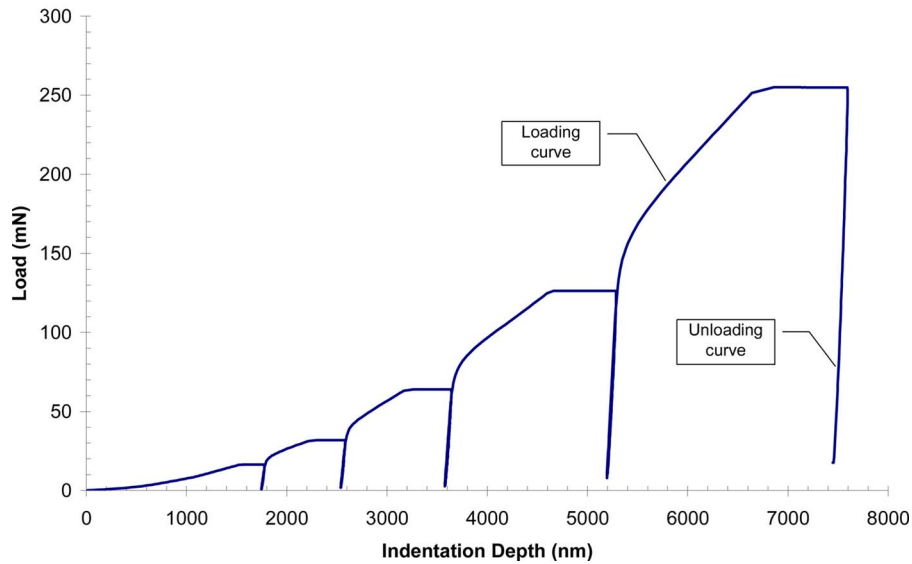


Fig. 10 A typical load/unloading curve for an indentation point. The curve is used to determine the hardness and elastic modulus.

Hardness of Specimen 1 for TG 712h Sample at Distance 0.95

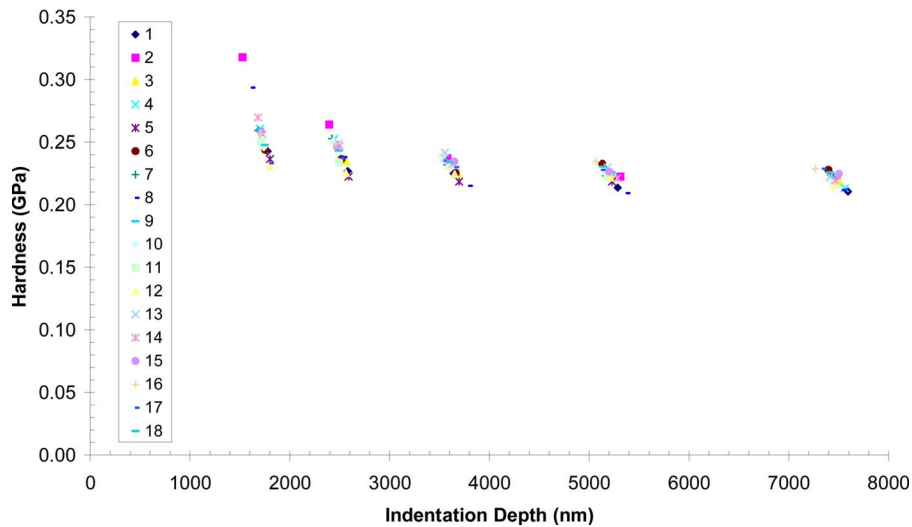


Fig. 11 A plot of hardness versus indentation depth for specimen 1 for the thermal gradient experiment after 712 h at a normalized distance of 0.95 from the hot side

Elastic Modulus of Specimen 1 for TG 712h Sample at Distance 0.95

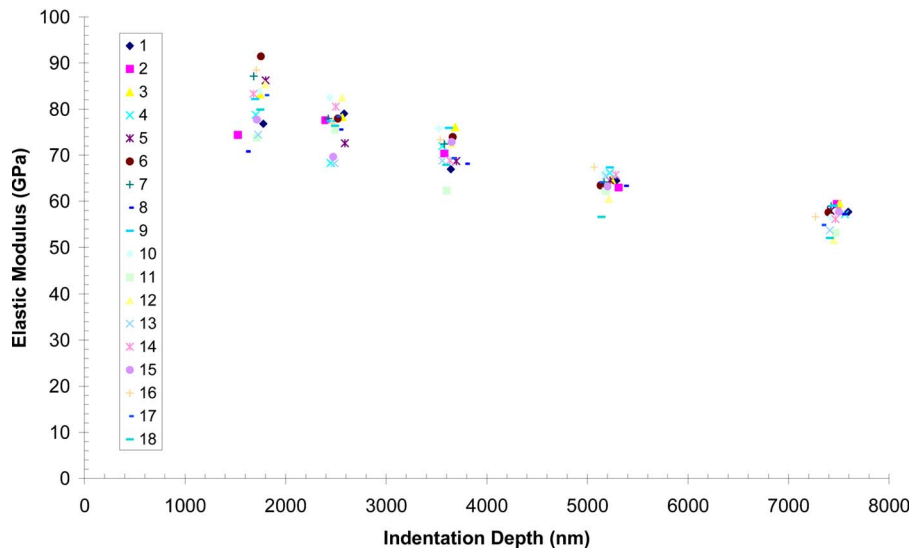


Fig. 12 A plot of elastic modulus versus indentation depth for specimen 1 for thermal gradient experiment after 712 h at a normalized distance of 0.95 from the hot side

erence, and has a value of 0.21 ± 0.01 GPa. This value is identical to the value, which is 0.21 ± 0.03 GPa, obtained by Ye [1] for the SnPb solder. The average hardness for isothermal (IT) samples is relatively constant, and lower than the TG samples. Structural changes for the isothermal samples all occurred within the first test interval of 286 h.

The average elastic modulus (Fig. 14) for the thermal gradient and isothermal samples remains relatively constant across the

surface area, except for moderate variations during the 286 h samples. In all cases, the elastic moduli do not show any change in value toward the cold side. The median value for the elastic modulus based on all tested samples is 55.1 ± 7.5 GPa. Elastic properties of SnPb solder alloys have been studied extensively, and a detailed review is given by Basaran and Jiang [20]. For comparison, elastic moduli for some lead-free and tin lead solders are presented in Table 5.

Average Measured Hardness for Isothermal and Thermal Gradient Samples

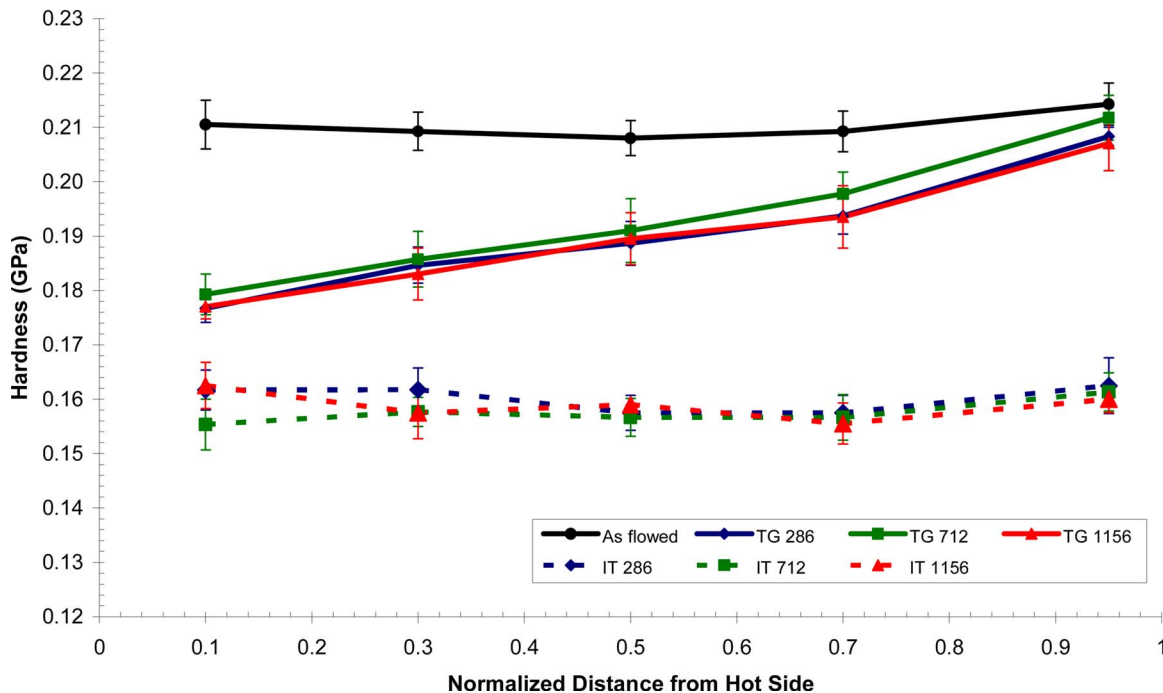


Fig. 13 Average measured surface hardness of thermomigration and isothermal samples across the solder height (TG: thermal gradient, IT: isothermally annealing)

Average Calculated Modulus for Isothermal and Thermal Gradient Samples

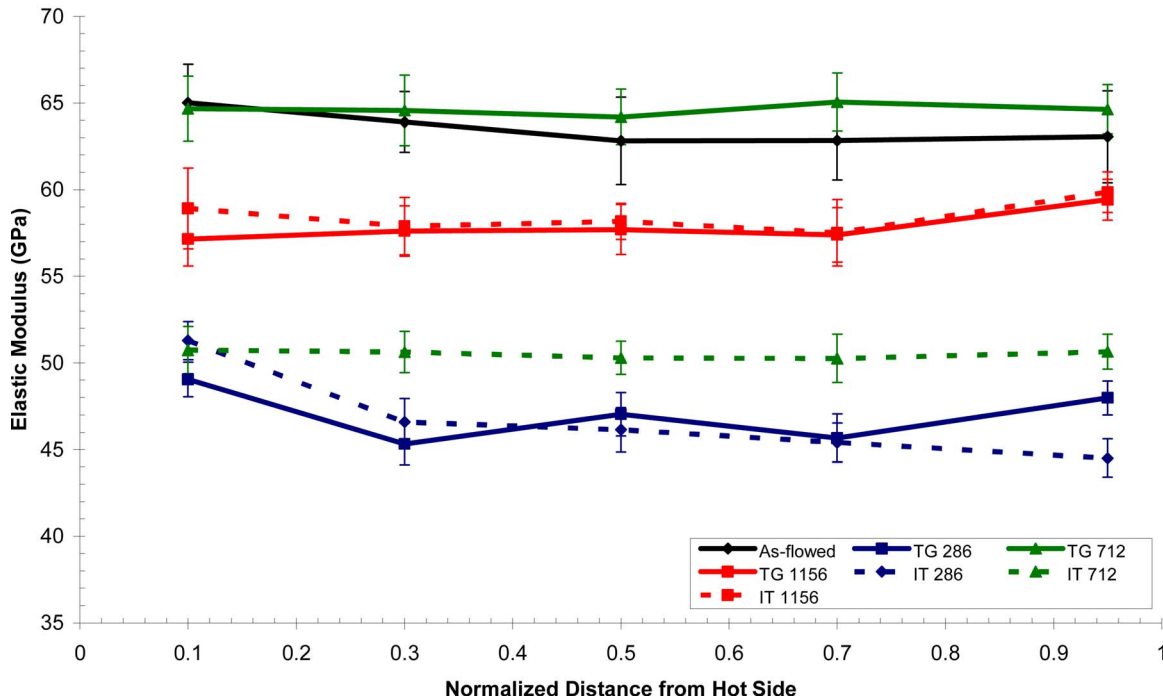


Fig. 14 Average calculated elastic modulus of thermomigration and isothermal samples across the solder height (TG: thermal gradient, IT: isothermally annealing)

5 Discussion

The two major microstructural differences observed between thermomigration and isothermal experiments are (1) the absence of Cu_3Sn at both the cold and hot sides in thermomigration samples, and (2) the thinning of Cu_6Sn_5 layer on the hot (155°C) side in thermomigration samples.

The thinning of as-flowed Cu_6Sn_5 IMC layer at the hot side is due its disintegration to 6Cu and 5Sn atoms under thermal gradient according to Eq. (1)



The Soret effect from thermal gradient segregates the Cu_6Sn_5 IMC to Sn- and Cu-rich layers, as shown in Fig. 15(a). The Cu atoms from the Cu-rich layer drift to the cold side under the thermal gradient force. A similar result was observed by Ding et al. [23,24] under electromigration at 150°C isothermal temperature. They conclude that Cu atoms from Cu-UBM and Cu_6Sn_5 dissolutions drift to bulk solder under electromigration force.

Since a Cu atom is lighter (atomic mass of 63.5 g/mol and atomic radius of 1350 \AA) than the Sn atom (118.7 g/mol and 1450 \AA), and being the dominant diffusion species [13], Cu atoms move faster to the cold side under the thermal gradient driving force. The diffusivity rates, $D_{\text{Cu-in-Sn}}$ and $D_{\text{Sn-in-Sn}}$ at 20°C are $3.09 \times 10^{-13} \text{ m}^2/\text{s}$ and $1.78 \times 10^{-17} \text{ m}^2/\text{s}$, respectively; at 190°C , $D_{\text{Cu-in-Sn}}$ and $D_{\text{Sn-in-Sn}}$ are $4.49 \times 10^{-11} \text{ m}^2/\text{s}$ and 1.33

$\times 10^{-14} \text{ m}^2/\text{s}$ [25]. Cu diffusivity is 4 orders of magnitude faster than Sn diffusivity at 20°C , and 3 at 190°C . This difference in migration speed produces segregation effect, in which Cu is seen to migrate to the cold side while Sn to the other, which is consistent with previous studies [5,26].

The apparent movement of Cu to the cold side and Sn to hot side is caused by the different rates of diffusivity. Under thermal gradient force, both atoms move to the cold side. Since Cu has a higher rate of diffusivity than Sn, Cu will move faster than Sn to the cold side. In the long run, this difference in diffusivity rate segregates Cu and Sn atoms. A high concentration of Cu can be seen on the cold side, while Sn on the hot side.

While Cu atoms are seen to migrate to the cold side, Sn atoms from the disintegration react with Cu atoms from the plate to form a new thin layer of Cu_6Sn_5 , as shown in Fig. 15(c). This new Cu_6Sn_5 IMC layer maintains the bond between the Cu plate and the solder joint. Since the Cu plate provides unlimited Cu atoms, there will always be a thin layer of Cu_6Sn_5 layer. The layer terminal thickness is governed by the rate of dissolution of "old" and formation of "new" Cu_6Sn_5 IMC. In this experiment, the thickness is about $3.1 \pm 0.8 \text{ \mu m}$. If the supply of Cu atom is limited, such as in the case of a thin Cu-UBM, there will be no Cu_6Sn_5 after sometime. This depletion of Cu atom from Cu-UBM and Cu dissolution from Cu_6Sn_5 create a gap between the UBM and solder bulk thus creating reliability issues. If the IMC layer is too thin, there will be no adhesion between the Cu plate and solder bulk [27], while too thick a layer will decrease fracture toughness [28,29].

Since Sn is highly reactive with Cu, a normal practice in the industry is to have a Ni coating on the Cu pad before Sn rich solder joint is attached. Ni coating not only helps in preventing oxidation and corrosion, but also serves as a diffusion barrier [30].

In the isothermal case, Cu_3Sn is formed between Cu plate and Cu_6Sn_5 layer, which is similar to earlier studies [31,32] for isothermal aging between 100°C and 350°C . Deng et al. [33] suggested that the Cu_3Sn growth is due to the reaction of Cu with

Table 5 Elastic moduli for some lead-free and tin lead solders

Solder	Elastic modulus (GPa)	Reference
Sn-3.5Ag	56	[21]
Sn-5Sb	58	[21]
Sn-2.5Ag-0.8Cu-0.5Sb (Castin™)	51.2	[22]
Sn-37Pb	9-48	[20]

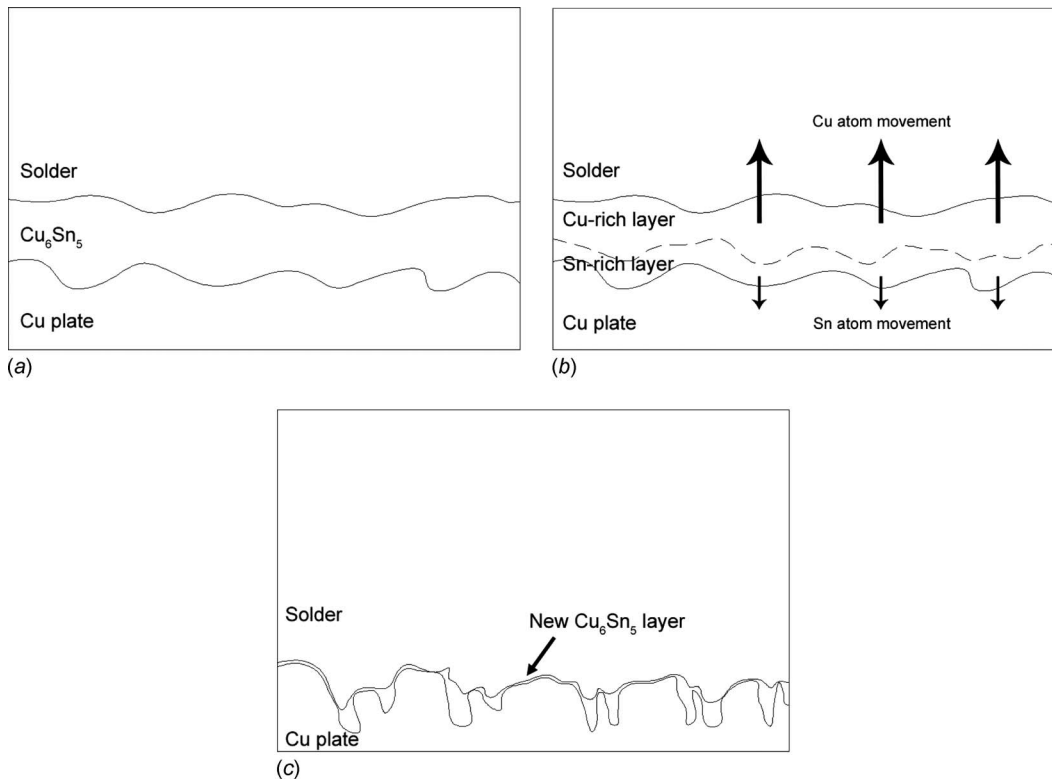


Fig. 15 The process of “old” Cu_6Sn_5 layer disintegration into “new” layer of Cu_6Sn_5

Cu_6Sn_5 , according to Eq. (2), while Zeng et al. [34] argued that the growth is due to either the reaction of Sn and Cu, or decomposition of Cu_6Sn_5 , according to Eq. (3). The reaction requires one Sn and three Cu atoms, while the decomposition of Cu_6Sn_5 releases two Cu_3Sn molecules and three Sn atoms [34].



At the hot side in the thermal gradient case, there is no observable Cu_3Sn IMC. Even though the supply of both Cu from the plate and Sn from the solder is abundant, the required mass concentration combination is not achieved to form Cu_3Sn in the thermal gradient samples. At the hot end, the required mass concentration of both Cu and Sn, about 39% and 61%, respectively, to form Cu_6Sn_5 is achieved. The required mass concentration to form Cu_3Sn is about 62% Cu and 38% Sn. This is achieved in isothermal samples but is not achieved in thermal gradient samples indicating that, while some Cu atoms reacted with Sn atoms to form a “new” Cu_6Sn_5 , as discussed in an earlier paragraph, the other drifted to the cold side under thermal gradient force.

While the cold (55°C) side of the thermomigration sample is not favorable for Cu_3Sn IMC formation, the excess Cu coming

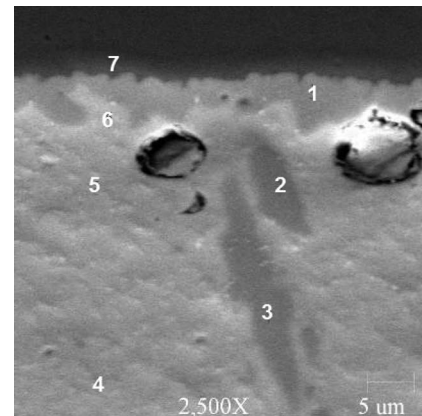


Fig. 16 SEM image of the cold interface after 712 h. Points 1–3 are identified as the Cu_6Sn_5 IMC. Points 4–6 show the increase in Cu concentration as points are closer to the interface.

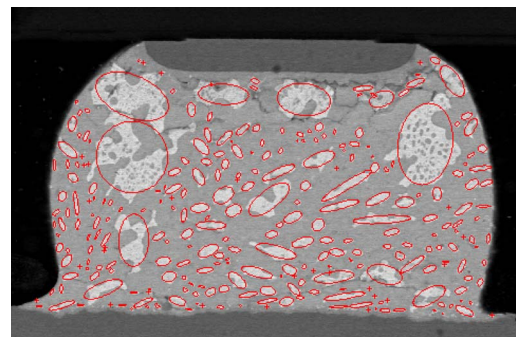


Fig. 17 Pb-grain coarsening reported by Ye et al [36]. At the chip (hot) side, the Pb-grain size is larger compared with the substrate (cold) side.

Table 6 Element analysis near the cold interface after 712 h

Point	Sn (wt %)	Ag (wt %)	Cu (wt %)
1	67.7	0.0	32.3
2	64.7	0.5	34.8
3	64.3	0.0	35.7
4	97.2	2.4	0.4
5	96.4	2.8	0.8
6	93.4	0.1	6.5
7	0.3	0.2	99.5

Table 7 Numerical data and statistical analysis for Figs. 11 and 12

Indentation no.	Data at maximum load			
	Hardness (GPa)	Modulus (GPa)	Depth (nm)	Load (mN)
1	0.210	57.731	7593.750	253.224
2	0.219	59.411	7480.330	255.797
3	0.218	59.558	7506.897	256.669
4	0.213	57.201	7561.232	254.262
5	0.222	57.942	7417.744	254.394
6	0.228	57.595	7397.745	259.738
7	0.220	58.944	7422.967	252.832
8	0.212	57.247	7537.265	250.913
9	0.223	59.040	7447.859	257.588
10	0.219	56.543	7419.871	251.568
11	0.216	53.181	7469.431	251.319
12	0.215	51.529	7450.361	248.829
13	0.223	53.751	7411.852	254.667
14	0.219	56.170	7466.643	254.963
15	0.225	57.733	7501.196	263.625
16	0.229	56.651	7268.164	251.765
17	0.229	54.858	7336.099	256.172
18	0.226	52.063	7411.301	258.006
Mean	0.220	56.508	7450.039	254.796
Std. dev.	0.006	2.466	77.645	3.565
% COV	2.55	4.36	1.04	1.40

from the hot side reacts with existing Cu₆Sn₅ IMC to form finger-like Cu₆Sn₅. An EDX analysis near the cold side (points 4–6) after 712 h shows high concentration of Cu, as shown in Table 6 and Fig. 16.

Under the thermal gradient, the hardness shows an increasing trend from the hot to the cold side, while the elastic modulus remains relatively unchanged. In the isothermal case, both the hardness and elastic modulus remain relatively constant. The hardness degradation from the cold side to the hot side in the thermomigration samples could be theoretically attributed to the Sn-grain coarsening from the cold to the hot side.

Grain size and hardness degradation from the cold to the hot side can be explained using the Hall–Petch relation for hardness [35]

$$H_v = H_O + k_H d^{-1/2} \quad (4)$$

where H_O and k_H are material constants, and d is grain diameter. A smaller grain size at the cold side means more grain boundaries, which act as dislocation motion barriers. As motion is impeded, stresses required to continue the deformation process increase [36], as a result, the material has a greater hardness. For isothermal samples, the grain size is uniform across the solder joint according to this relation, and accordingly no change in hardness. Further work is required to substantiate this, but for the SnPb solder, nanoindentation results from Ref. [37] show that the mechanical properties are in agreement with the Hall–Petch relation. They observed Pb-grain coarsening after thermomechanical loading, and found that solder alloy properties degrade from the substrate (cold) to the chip (hot) side. Investigation of Pb-grain size shows that the grain is larger at the hot side than at the cold side, as shown in Fig. 17.

Table 8 Average measured hardness from nanoindentation tests

Distance	Specimen no.	Average measured hardness (GPa)						
		As-flowed	Thermal gradient (TG)				Isothermal (IT)	
		0 h	286 h	712 h	1156 h	286 h	712 h	1156 h
0.10	1	0.192	0.188	0.179	0.182	^a	0.156	0.164
	2	0.225	0.175	0.182	0.172	0.175	0.155	0.161
	3	0.222	0.167	0.181		0.152	0.155	
	4	0.203		0.175		0.158		
	Mean	0.211	0.177	0.179	0.177	0.162	0.155	0.163
0.30	1	0.196	0.199	0.191	0.185	0.158	0.158	0.155
	2	0.218	0.181	0.181	0.181	0.171	0.157	0.160
	3	0.224	0.174	0.187		0.158	0.158	
	4	0.199		0.184		0.160		
	Mean	0.209	0.185	0.186	0.183	0.162	0.158	0.158
0.50	1	0.197	0.200	0.200	0.187	0.152	0.156	^a
	2	0.214	0.187	0.182	0.192	0.171	0.162	0.159
	3	0.220	0.179	0.193		0.155	0.152	
	4	0.201		0.189		0.152		
	Mean	0.208	0.189	0.191	0.190	0.158	0.157	0.159
0.70	1	0.197	0.208	0.206	0.189	0.154	0.155	0.154
	2	0.210	0.190	0.193	0.198	0.172	0.163	0.157
	3	0.223	0.183	0.195		0.150	0.152	
	4	0.207		0.197		0.154		
	Mean	0.209	0.194	0.198	0.194	0.158	0.157	0.156
0.95	1	0.199	0.224	0.220	0.201	0.171	0.167	0.160
	2	0.206	0.203	0.205	0.213	0.174	0.159	0.160
	3	0.241	0.198	0.207		0.147	0.158	
	4	0.211		0.215		0.158		
	Mean	0.214	0.208	0.212	0.207	0.163	0.161	0.160
Total specimen		4	3	4	2	4	3	2

^aWrong test parameter applied.

Table 9 Average calculated modulus from nanoindentation tests

Distance	Specimen no.	Average calculated modulus (GPa)						
		As-flowed	Thermal gradient (TG)			Isothermal (IT)		
		0 h	286 h	712 h	1156 h	286 h	712 h	1156 h
0.10	1	60.7	65.7	56.2	52.8	^a	62.0	57.6
	2	61.8	38.6	73.4	61.5	67.1	45.0	60.2
	3	75.4	42.8	68.4		42.3	45.2	
	4	62.1		60.7		44.4		
	Mean	65.0	49.0	64.7	57.2	51.3	50.7	58.9
0.30	1	56.5	63.1	56.3	53.9	41.5	62.3	57.1
	2	59.8	30.4	73.9	61.3	61.8	46.3	58.7
	3	74.7	42.5	68.1		42.0	43.3	
	4	64.7		59.9		41.1		
	Mean	63.9	45.3	64.6	57.6	46.6	50.6	57.9
0.50	1	52.1	63.1	56.6	54.0	40.7	61.8	^a
	2	61.4	34.7	71.7	61.4	61.0	46.4	58.2
	3	71.9	43.3	67.8		43.2	42.7	
	4	65.9		60.6		39.6		
	Mean	62.8	47.0	64.2	57.7	46.1	50.3	58.2
0.70	1	52.6	63.0	56.9	54.2	40.3	62.0	55.6
	2	61.4	30.3	72.3	60.6	59.8	46.7	59.5
	3	71.4	43.7	69.3		41.6	42.1	
	4	66.0		61.8		39.9		
	Mean	62.8	45.7	65.1	57.4	45.4	50.3	57.5
0.95	1	52.4	63.2	56.5	54.0	33.1	65.4	59.4
	2	57.0	34.5	72.5	64.9	61.4	45.4	60.3
	3	72.7	46.2	68.6		42.8	41.2	
	4	70.2		60.9		40.8		
	Mean	63.1	48.0	64.6	59.4	44.5	50.6	59.9
Total specimen		4	3	4	2	4	3	2

^aWrong test parameter applied.

6 Conclusions

The microstructural and mechanical properties of the lead-free solder joint/copper pad interface were studied under a thermal gradient of 1000°C/cm. The two major microstructure differences between the thermomigration and isothermal samples are the lack of Cu₃Sn IMC layer at both the hot and cold sides and the thinning of Cu₆Sn₅ IMC layer at the hot side under thermal gradient driving force.

In the thermomigration samples, the thinning of Cu₆Sn₅ layer is a result of its disintegration, while the absence of Cu₃Sn IMC layer is a result of insufficient Cu mass concentration to form Cu₃Sn layer. The samples form only Cu₆Sn₅ IMC and show more Cu concentration near the cold side, which resulted in a well defined Cu₆Sn₅/solder interface.

In the isothermal annealing case, Cu₃Sn layer is formed between the Cu plate and Cu₆Sn₅ layer. The Cu₆Sn₅ layer thickness is about 2.3 that of Cu₃Sn layer over time, suggesting that the growth rate of Cu₆Sn₅ is faster than that of Cu₃Sn.

Under thermal gradient driving force, the hardness degradation from the cold to the hot side could be attributed to Sn-grain coarsening at the hot side. Hardness degradation was not observed across the solder joint for isothermal aging samples, which indicates uniformity in Sn-grain size. Further work is required to verify this.

Acknowledgment

This project has been partly sponsored by U.S. Navy Office of Naval Research Advanced Electrical Power Systems under the direction of Terry Ericson.

Appendix

Numerical data and statistical analysis for Figs. 11 and 12 are presented in Table 7. The averaged measured hardness and average calculated modulus from nanoindentation tests are presented in Tables 8 and 9, respectively.

References

- [1] Ye, H., 2004, "Mechanical Behavior of Microelectronics and Power Electronics Solder Joints Under High Current Density: Analytical Modeling and Experimental Investigation," Ph.D. thesis, State University of New York at Buffalo.
- [2] Ye, H., Basaran, C., and Hopkins, D. C., 2003, "Damage Mechanics of Microelectronics Solder Joints Under High Current Densities," *Int. J. Solids Struct.*, **40**(15), pp. 4021–4032.
- [3] Basaran, C., Lin, M., and Ye, H., 2003, "A Thermodynamic Model for Electrical Current Induced Damage," *Int. J. Solids Struct.*, **40**(26), pp. 7315–7327.
- [4] Basaran, C., Ye, H., and Hopkins, D. C., 2005, "Failure Modes of Flip Chip Solder Joints Under High Electric Current Density," *ASME J. Electron. Packag.*, **127**(2), pp. 157–163.
- [5] Huang, A. T., Gusak, A. M., Tu, K. N., and Lai, Y.-S., 2006, "Thermomigration in SnPb Composite Flip Chip Solder Joints," *Appl. Phys. Lett.*, **88**(14), pp. 141911–141913.
- [6] Ye, H., Basaran, C., and Hopkins, D., 2003, "Thermomigration in Pb–Sn Solder Joints Under Joule Heating During Electric Current Stressing," *Appl. Phys. Lett.*, **82**(7), pp. 1045–1047.
- [7] Ye, H., Basaran, C., and Hopkins, D. C., 2003, "Mechanical Degradation of Microelectronics Solder Joints Under Current Stressing," *Int. J. Solids Struct.*, **40**(26), pp. 7269–7284.
- [8] Ye, H., Hopkins, D. C., and Basaran, C., 2003, "Measurement of High Electrical Current Density Effects in Solder Joints," *Microelectron. Reliab.*, **43**(12), pp. 2021–2029.
- [9] Soret, C., 1879, "Sur L'état D'équilibre Que Prend Au Point De Vue De Sa Concentration Une Dissolution Saline Primitivement Homohéne Dont Deux Parties Sont Portées À Des Températures Différentes," *Arch. Sci. Phys. Nat.*, **2**, pp. 48–61.

- [10] Platten, J. K., 2006, "The Soret Effect: A Review of Recent Experimental Results," *ASME J. Appl. Mech.*, **73**(1), pp. 5–15.
- [11] Roush, W., and Jaspal, J., 1982, "Thermomigration in Lead-Indium Solder," *Electronic Components Conference*, San Diego, CA, Vol. 32, pp. 342–345.
- [12] 2004, "Moisture/Reflow Sensitivity Classification for Nonhermetic Solid State Surface Mount Devices," JEDEC Solid State Association and IPC, Report No. IPC/JEDEC J-STD-020C.
- [13] Tu, K. N., 1973, "Interdiffusion and Reaction in Bimetallic Cu–Sn Thin Films," *Acta Metall.*, **21**(4), pp. 347–354.
- [14] Oliver, W. C., and Pharr, G. M., 1992, "An Improved Technique for Determining Hardness and Elastic Modulus Using Load and Displacement Sensing Indentation Experiments," *J. Mater. Res.*, **7**(6), pp. 1564–1569.
- [15] 2007, "Engineering Fundamentals: Element Listing," http://www.efunda.com/materials/elements/element_list.cfm
- [16] 2004, "Review and Analysis of Lead-Free Solder Material Properties," http://www.metallurgy.nist.gov/solder/clech/Sn-Ag-Cu_Other.htm
- [17] 2007, "Specialty Solder and Alloys Technical Information," <http://www.indium.com/products/alloychart.php>
- [18] Grusd, A., 1998, "Lead Free Solders in Electronics," *Surface Mount International Conference*, San Jose, CA.
- [19] Lee, T. Y., and Choi, W. J., 2002, "Morphology, Kinetics, and Thermodynamics of Solid-State Aging of Eutectic SnPb and Pb-Free Solders (Sn–3.5Ag, Sn–3.8Ag–0.7Cu and Sn–0.7Cu) on Cu," *J. Mater. Res.*, **17**(2), pp. 291–301.
- [20] Basaran, C., and Jiang, J., 2002, "Measuring Intrinsic Elastic Modulus of Pb/Sn Solder Alloys," *Mech. Mater.*, **34**(6), pp. 349–362.
- [21] McCabe, R. J., and Fine, M. E., 1998, "Athermal and Thermally Activated Plastic Flow in Low Melting Temperature Solders at Small Stresses," *Ser. Mater.*, **39**(2), pp. 189–195.
- [22] Seelig, K., and Suraski, D., 2000, "The Status of Lead-Free Solder Alloys," *Proceedings of the 50th Electronic Components and Technology Conference*, pp. 1405–1409.
- [23] Ding, M., Wang, G., Chao, B., Ho, P. S., Su, P., and Trent, U., 2006, "Effect of Contact Metallization on Electromigration Reliability of Pb-Free Solder Joints," *J. Appl. Phys.*, **99**(9), p. 094906.
- [24] Ding, M., Wang, G., Chao, B., Ho, P. S., and Su, P., 2005, "A Study of Electromigration Failure in Pb-Free Solder Joints," *Proceedings of the 43rd IEEE International Reliability Physics Symposium*, pp. 518–523.
- [25] Mei, Z., Sunwoo, A. J., and Morris, J. W., Jr., 1992, "Analysis of Low-Temperature Intermetallic Growth in Copper-Tin Diffusion Couples," *Metall. Trans. A*, **23A**(3), pp. 857–864.
- [26] Schroerschwartz, R., and Heitkamp, D., 1971, "Thermotransport of Substitutional Impurities in Copper," *Phys. Status Solidi B*, **45**(1), pp. 273–286.
- [27] Tu, K. N., and Zeng, K., 2001, "Tin-Lead (SnPb) Solder Reaction in Flip Chip Technology," *Mater. Sci. Eng. R.*, **34**(1), pp. 1–58.
- [28] Pratt, R. E., Stromswold, E. I., and Quesnel, D. J., 1996, "Effect of Solid-State Intermetallic Growth on the Fracture Toughness of Cu/63Sn-37Pb Solder Joints," *IEEE Trans. Compon., Packag., Manuf. Technol., Part A*, **19**(1), pp. 134–141.
- [29] Abdulhamid, M., Basaran, C., and Lai, Y. S., "Thermomigration vs. Electromigration in Lead Free Solder Alloys," *IEEE Trans. On Advanced Packaging* (to be published).
- [30] Fu, R., Liu, L., Liu, D., and Zhang, T.-Y., 2006, "In Situ Formation of Cu–Sn–Ni Intermetallic Nanolayer as a Diffusion Barrier in Preplated Lead Frames," *Appl. Phys. Lett.*, **89**(13), pp. 131911–131913.
- [31] Tu, K. N., and Thompson, R. D., 1982, "Kinetics of Interfacial Reaction in Bimetallic Cu–Sn Thin Films," *Acta Metall.*, **30**(5), pp. 947–952.
- [32] Yoon, J.-W., and Lee, Y.-H., 2004, "Intermetallic Compound Layer Growth at the Interface between Sn–Cu–Ni Solder and Cu Substrate," *J. Alloys Compd.*, **381**(1–2), pp. 151–157.
- [33] Deng, X., Piotrowski, G., Williams, J. J., and Chawla, N., 2003, "Influence of Initial Morphology and Thickness of Cu₆Sn₅ and Cu₃Sn Intermetallics on Growth and Evolution During Thermal Aging of Sn–Ag Solder/Cu Joints," *J. Electron. Mater.*, **32**(12), pp. 1403–1413.
- [34] Zeng, K., Stierman, R., Chiu, T. C., Edwards, D., Ano, K. C., and Tu, K. N., 2005, "Kirkendall Void Formation in Eutectic SnPb Solder Joints on Bare Cu and Its Effect on Joint Reliability," *J. Appl. Phys.*, **97**(2), p. 024508.
- [35] Tjong, S. C., and Chen, H., 2004, "Nanocrystalline Materials and Coatings," *Mater. Sci. Eng. R.*, **45**, pp. 1–88.
- [36] Hall, E. O., 1951, "The Deformation and Aging of Mild Steel. III. Discussion of Results," *Proc. Phys. Soc. London*, **B64**, pp. 747–753.
- [37] Ye, H., Basaran, C., and Hopkins, D. C., 2004, "Pb Phase Coarsening in Eutectic Pb/Sn Flip Chip Solder Joints Under Electric Current Stressing," *Int. J. Solids Struct.*, **41**(9–10), pp. 2743–2755.